



Subsidence prediction of a rubble mound breakwater at Yantai port: A application of FSSI-CAS 2D

Jianhong Ye ^{a,*}, Kunpeng He ^{a,b}, Lijie Zhou ^a

^a State Key Laboratory of Geomechanics and Geotechnical Engineering, Institute of Rock and Soil Mechanics, Chinese Academy of Sciences, Wuhan 430071, China

^b University of Chinese Academy of Sciences, Beijing 100049, China

ARTICLE INFO

Keywords:

FSSI-CAS 2D
Modified Cambridge clay model
Numerical modeling
Poro-elastic model
Rubble mound breakwater
Subsidence
Yantai port

ABSTRACT

This study is an application of the integrated numerical model FSSI-CAS 2D, to predict the subsidence of a huge rubble mound breakwater in the west part zone at Yantai port. The modified Cambridge clay soil model and poro-elastic model are adopted to describe the quasi-static mechanical behavior of the seabed foundation, which consists of muddy-clay, clay and silt soil layers. The model parameters of soil used in computation are estimated based on a great number of laboratory tests (over one thousand). A novel point is that the buoyancy applied on the rubble mounds under SWL (Static Water Line), as well as its nonlinear variation dependent on the deformation of seabed foundation are considered in computation. Through analytical and experimental verification, as well as the comparison with observation data monitored in-situ, it is indicated that FSSI-CAS 2D is reliable to numerically predict the subsidence of offshore structures, and has the ability to be applied in practical engineering.

1. Introduction

It is well known that the geological deposition history of offshore seabed foundation soil generally is relatively short due to the rapid depositing rate in offshore environment (Daigle et al., 2017). Most of offshore seabed foundation has the characteristics of less density and relatively low bearing capacity (Anderson, 2009). After constructed on this type of seabed foundation, significant post-construction subsidence would occur for offshore structures (Shen et al., 2017; Setan and Othman, 2006). Meanwhile, the seabed soil beneath structures will be compressed to a dense state. Excessive subsidence itself is not necessarily harmful for the ability of offshore structures. However, whether the magnitude of subsidence is accurately predicted or not would have an extremely important effect on the normal service performance of offshore structures after construction. In the practice of engineering, some redundant height generally will be reserved for offshore structures in design stage, to counteract the effect of the post-construction subsidence, guaranteeing the working surfaces reaching the designed elevation in their service phase. Therefore, the accurate prediction of the post-construction subsidence of structures is considerably crucial for the structure design and the normal service performance of offshore structures.

The subsidence of offshore structures could be caused by the wave/current-induced scouring (Fazeres-Ferradosa et al., 2018, 2020), and by the dynamic loading, e.g. seismic wave or ocean wave, as

well as the structures weight-induced static loading. Subsidence of offshore structure caused by dynamic loading is certainly due to the liquefaction-post consolidation process of seabed foundation (Karamitros et al., 2013; Konagai et al., 2013; Verdugo and Gonzalez, 2015; Sumer et al., 2007; Ye and Wang, 2015; Ye et al., 2017). However, the subsidence caused by the weight of structures will be the focus in this study. The layer wise summation method proposed by a series of national codes, e.g. Chinese Code for Investigation of Geotechnical Engineering (GB50021-2001), is widely adopted by engineers to predict the post-construction subsidence of offshore structures. It is worth to point out that this method is based on the concept of linear elasticity, considering that seabed foundation soil is linear elastic material. However, the deformation behavior of real seabed soil is complicatedly nonlinear, rather than simply linear elastic. Therefore, layer wise summation method is a type of semi-theory and semi-experiences method. The credibility of the results given by this method is general. This is the reason why the subsidence of structures predicted by the layer wise summation method needs a second empirical correction in practical engineering. Even so, the final predicted subsidence by this method would frequently be significantly different with the in-site monitoring results.

Apart from semi-theory, semi-experiences method, another is the theoretical approach. Generally, Biot's consolidation equation, and advanced soil constitutive models, e.g. Cambridge clay model, that could

* Corresponding author.

E-mail address: Jhye@whrsm.ac.cn (J. Ye).

describe the complicated mechanical behavior of soil foundation, are taken to predict the deformation of seabed foundation, and the post-construction subsidence of overlying offshore structures. To the author's best knowledge, there are only few works are available so far. Ye (2012b), Jeng and Ye (2012), Shen et al. (2017), and Ye et al. (2012) studied the post-construction subsiding process of large-scale offshore breakwaters, and the consolidation characteristics of their seabed foundation adopting the numerical model FSSI-CAS 2D/3D. Their works have improved the understanding of the subsidence problem of offshore structures. However, the above mentioned previous works were only performed specially for some idea conditions in which simple topography and structure configuration, and pore-elasticity were involved. There was basically no a work has been conducted for a complicated practical engineering case in which real complex topography of seabed floor, and complex nonlinear constitutive soil model were involved. The integrated numerical model FSSI-CAS 2D is an unique computation model. It not only can be applied to the problem of fluid–structure–seabed foundation interaction (Ye et al., 2013, 2014, 2015), and the seismic dynamics of offshore structure and its seabed foundation (Ye and Wang, 2015, 2016), but also can be applied to the problem of seabed consolidation and the subsidence of offshore structures (Ye, 2012b; Jeng and Ye, 2012; Ye et al., 2012). Specially, the hydrostatic pressure applied by seawater on seabed floor and outer surface of offshore structures, as well as the buoyancy applied to structures and its variation dependent on the deformation of seabed foundation can be effectively taken into consideration in computation by FSSI-CAS 2D, detailed information please see Ye et al. (2012). However, the above two factors are frequently difficult to be handled by other commercial or open source packages due to the fact that a wave model for the hydrostatic and hydrodynamics of seawater is generally not included in them. This priority reflects that FSSI-CAS 2D is worth to be used in the field of offshore geotechnics.

In this study, in order to apply FSSI-CAS 2D into engineering practice, taking the rubble mound breakwater in the west port zone at Yantai port as the engineering background, the integrated numerical model FSSI-CAS 2D is adopted as the computation tool, the weight-induced post-construction subsidence of a large-scale rubble mound breakwater will be predicted considering the soil layers division and the mechanical parameters obtained through in-situ geotechnical engineering investigation and laboratory tests. Comparison analysis finds that the numerically predicted result is basically anastomotic to the in-situ monitoring data. It is indicated that FSSI-CAS 2D is feasible for the engineering problem of subsidence prediction of offshore breakwater. This works presented in this study can provide an application case of FSSI-CAS 2D for the purpose of referencing.

2. Numerical model and constitutive model

Dynamic Biot's equation known as “ $u - p$ ” approximation proposed by Zienkiewicz et al. (1980) are used to govern the consolidation behavior of seabed foundation, as well as the subsidence behavior of offshore structures:

$$\frac{\partial \sigma'_x}{\partial x} + \frac{\partial \tau_{xz}}{\partial z} = -\frac{\partial p}{\partial x} + \rho \frac{\partial^2 u_s}{\partial t^2}, \quad (1)$$

$$\frac{\partial \tau_{xz}}{\partial x} + \frac{\partial \sigma'_z}{\partial z} + \rho g = -\frac{\partial p}{\partial z} + \rho \frac{\partial^2 w_s}{\partial t^2}, \quad (2)$$

$$k \nabla^2 p_s - \gamma_w n \beta \frac{\partial p}{\partial t} + k \rho_f \frac{\partial^2 \epsilon_v}{\partial t^2} = \gamma_w \frac{\partial \epsilon_v}{\partial t}, \quad (3)$$

where u_s, w_s are the soil displacements in horizontal and vertical direction, respectively; n is soil porosity; σ'_x and σ'_z is effective normal stresses in the horizontal and vertical direction, respectively (Noted: compressive stress is taken as negative in this study); τ_{xz} is shear stress; p is the pore water pressure; $\rho = \rho_f n + \rho_s(1 - n)$ is the average density of

porous seabed; ρ_f is the fluid density; ρ_s is solid density; k is the Darcy's permeability; g is the gravitational acceleration, γ_w is unit weight of water and ϵ_v is the volumetric strain. In Eq. (3), the compressibility of pore fluid (β) and the volumetric strain (ϵ_v) are defined as

$$\beta = \left(\frac{1}{K_f} + \frac{1 - S_r}{p_{w0}} \right), \quad \text{and} \quad \epsilon_v = \frac{\partial u_s}{\partial x} + \frac{\partial w_s}{\partial z}, \quad (4)$$

where S_r is the degree of saturation of seabed, p_{w0} is the absolute static pressure of pore water at a position, and K_f is the bulk modulus of pore water when $S_r=100\%$, generally, $K_f = 2.24 \times 10^9$ Pa. Here, the compressibility of pore fluid β is taken to consider the unsaturation of seabed soil, which is only applicable for the nearly saturated soil.

Finite element method (FEM) is utilized to solve the above governing equation (1) to (3), and Generalized Newmark Scheme (implicit scheme) is adopted to calculate the time integration when solving the above governing equations (Chan, 1988; Zienkiewicz et al., 1999). For the problem of Fluid–Structure–Seabed Interaction (FSSI), an integrated/coupled numerical model FSSI-CAS 2D was developed by the authors (Ye, 2012a). In FSSI-CAS 2D, the wave motion and the porous flow in porous seabed is governed by VARANS (Volume Average Reynolds Average Navier–Stokes) equation (Hsu et al., 2002). Meanwhile, the dynamic behavior of offshore structure and its seabed foundation is governed by the above Eqs. (1), (2) and (3). A coupled algorithm was developed to couple the VARANS equation and Biot's dynamics equation together. Actually, FSSI-CAS 2D has been widely verified by analytical solutions, a series of physical wave flume tests (Ye et al., 2013). More detailed information about the architecture and the reliability of FSSI-CAS 2D can be found in Ye et al. (2013) and Ye (2012a). Actually, comparing with other numerical model, such as ABAQUS, FLAC, the key advantages of FSSI-CAS 2D includes three aspects. Firstly, ‘ $u-p$ ’ approximation of Biot's equation is taken as the governing equation in the soil model, in which the acceleration term has been considered. As a result, FSSI-CAS 2D is not only can be used for consolidation problems, but also can be used for the problems of seismic dynamics of structures built on porous foundation in which pore water exists (Ye and Wang, 2015). However, the soil modulus in ABAQUS is not applicable for problems of seismic dynamics of structures built on porous foundation if there is pore water to our best knowledge. Secondly, two wave models, COBRAS and OLAFLOW for the hydrodynamics of all types of ocean waves have been integrated together with the soil model in FSSI-CAS 2D. As a result, FSSI-CAS 2D can be used to study the ocean waves-induced dynamics of offshore structures built on porous seabed foundation (Ye et al., 2014). So far as we know, these commercial software, such as ABAQUS, FLAC, ANASIS, PLAXIS all have no this function. Thirdly, even though there are also several integrated models developed based on OpenFoam (Li et al., 2020) or COMSOL MultiPhysics (Liao et al., 2018) so far; however, only poro-elastic soil model can be used in them. In FSSI-CAS 2D, a few elasto–plastic soil models, such as Drucker–Prager model, Mohr–Coulomb model, Modified Cambridge soil model, Pastor Zienkiewicz III model etc. have been available (Ye et al., 2015). Furthermore, the program interface for soil constitutive models also has been opened in FSSI-CAS 2D. As a consequence, the users can implant their own constitutive models developed by themselves through the dynamic-Link library technique. Overall, there are some unique advantages in FSSI-CAS 2D developed by ourselves.

Void ratio e and related Darcy's permeability k of soil generally is variational depending on the deformation of soil. In computation, the variation of void ratio of seabed soil is considered following $e_{n+1} = (1 + e_n) \exp(\frac{\Delta p}{Q} + \Delta \epsilon_{vs}) - 1$, which is established from the perspective of large deformation, where n stands for n th time step, Δp is the incremental pore pressure, $\Delta \epsilon_{vs}$ is the incremental volumetric strain of soil, and $Q = 1/\beta$ is the compressibility of pore water. Correspondingly, permeability of seabed soil k variates following $k = C_f \frac{e^3}{1+e}$, where $C_f = k_0 \frac{1+e_0}{e_0^3}$ is an empirical coefficient (Miyamoto et al., 2004), in which e_0 and k_0 is the initial void ratio and permeability. Additionally, the hydrostatic

water pressure acting on marine structure and its seabed foundation, as is the boundary values in FEM computation, is automatically variable based on the displacement of marine structures, and the deformation of seabed foundation. In the consolidation process, the void ratio of seabed foundation must reduce accompanying the pore water is drained out, leading to the subsidence of seabed foundation and its overlying marine structure. As a result, the hydrostatic pressure acting on structure and its seabed foundation would change significantly, especially in the cases involving large deformation.

3. Model validation

3.1. Analytical solution

There have been a series of analytical solutions for the soil consolidation problem in literature. Among them, the analytical solution proposed by Terzaghi (1925), and the one proposed by Mandel (1953) and Cryer (1963) are the most typical ones. It is noted that the validation for FSSI-CAS 2D by adopting the Terzaghi's solution has been previously conducted, see Ye (2012b) and Ye et al. (2012). Here, only the validation by adopting the analytical solution proposed by Mandel (1953) and Cryer (1963) is presented.

The typical Terzaghi's solution is actually a 1D solution for soil consolidation problem. While, the solution proposed by Mandel (1953) and Cryer (1963) is a 2D plane strain solution, as demonstrated in Fig. 1(a). A poro-elastic fully saturated medium, e.g. soil, is sandwiched by two rigid and impermeable plates; and this porous medium is compressed by the two plates on which two constant uniformly distributed pressure are applied reversely. The pore water in the poro-elastic medium can be freely drained out through the two lateral sides, resulting in the pore pressure on the lateral sides can be set as zero. The pore pressure will display a non-monotonic variation with consolidation time. At the initial consolidation time, an increase of the pore pressure will be induced near to the center of the rectangular medium. Subsequently, the pore pressure will dissipate normally. This phenomenon was firstly discovered and explained by Mandel (1953) and Cryer (1963), and was called as "Mandel-Cryer effect". The general solution to this Mandel-Cryer problem considering the compressibility of the poro-elastic medium was given by Cheng and Detournay (1988). The pore pressure p on the x axis is analytically expressed as:

$$p(x, t) = \frac{2FB(1 + \nu_u)}{3a} \sum_{i=1}^{\infty} \frac{\sin \alpha_i \cos \alpha_i}{\alpha_i - \sin \alpha_i \cos \alpha_i} (\cos \frac{\alpha_i x}{a} - \cos \alpha_i) \exp(-\frac{\alpha_i^2 c_v t}{a^2}) \quad (5)$$

$$\tan \alpha_i = \frac{1 - \nu}{\nu_u - \nu} \alpha_i \quad (6)$$

in which G is the shear modulus. ν and $\nu_u = \frac{3\nu + \alpha B(1-2\nu)}{3 - \alpha B(1-2\nu)}$ is the drained and undrained Poisson's ratio. $B = \frac{\alpha M}{K_u}$ is the Skempton coefficient, B is nearly 1.0 for fully saturated medium. $K_u = \lambda + 2\nu/3 + \alpha^2 M$ is the undrained bulk modulus. $M = [\frac{n}{K_f} + \frac{\alpha-n}{K_s}]^{-1}$ is the Biot modulus. n is the porosity. $\alpha = 1 - \frac{K_T}{K_s}$ is the Biot's coefficient. K_f is the bulk modulus of pure water, K_s is the bulk modulus of the particles making up the poro-elastic medium, and K_T is the overall bulk modulus of the poro-elastic medium, which is generally much less than K_s , resulting in α generally is very near to 1.0. $c_v = \frac{k}{\rho(M^{-1} + \alpha^2(\lambda + 2\nu)^{-1})}$ is the consolidation coefficient. ρ is the density of pore water. $\lambda = \frac{\nu E}{(1+\nu)(1-2\nu)}$, $\mu = G = \frac{E}{2(1+\nu)}$ are the Lamé's constant. E is the Young's modulus. a and b are the half of the length and height of the rectangular porous medium. $2F$ is the resultant force of the uniformly distributed pressure applied on the rigid plates. α_i ($i = 1, 2, 3, \dots, \infty$) are the roots of the nonlinear Eq. (6).

The integrated numerical model FSSI-CAS 2D is adopted to reproduce the pore pressure dissipation process at three typical position A

Table 1

Parameters used in the verification computation adopting Mandel's solution.			
Parameters	Value	Parameter	Value
E (MPa)	100	α	1.0
ν	0.25	n	0.375
ν_u	0.5	a (m)	20
λ (MPa)	40	b (m)	10
μ or G (MPa)	40	F (kN)	200
k (m/s)	1.0×10^{-5}	K_s (MPa)	1.0×10^6
B	0.9996	K_f (MPa)	2.24×10^3

($x = a/2, z = 0$), B ($x = 3a/4, z = 0$) and C ($x = 7a/8, z = 0$), as labeled in Fig. 1(a). The parameters of the poro-elastic medium used in this verification computation are listed in Table 1. The half length a and the half height b of the rectangular computational domain is 20 m and 10 m, respectively. The resultant force on the rigid plates is set as $F=200$ kN. It is noted that the gravity is not considered due to the fact that it is also not considered in the analytical solution. The comparison of the pore pressure dissipation process at position A, B and C between the numerical results predicted by FSSI-CAS 2D and the analytical solution proposed by Cheng and Detournay (1988) are shown in Fig. 1(b). It is observed that the numerical results predicted by FSSI-CAS 2D agree very well with the analytical solution. It is indicated that FSSI-CAS 2D is reliable for the consolidation problems.

3.2. Experimental test on clay soil

Nakai and Matsuoka (1986) has performed a series of triaxial test on the normally consolidated Fujinomori clay to verify the constitutive soil model proposed by them. Here, the conventional drained triaxial test data recorded by Nakai and Matsuoka (1986) are utilized to validate the modified Cambridge clay soil model in FSSI-CAS 2D, due to the fact that these test data given by Nakai and Matsuoka (1986) are very reliable, and the soil parameters also have been reliably calibrated by them. The soil parameters of the normally consolidation Fujinomori clay for the modified Cambridge model are: initial void ratio $e_0=0.7$, Poisson's ratio $\nu=0.3$, slope of normally compression line in $e-\ln p$ coordinates $\lambda=0.08636$, slope of rebound line in $e-\ln p$ coordinates $\kappa=0.01904$, slope of critical state line $M_f=1.4183$, overconsolidated ratio $OCR=1.0$. In FSSI-CAS 2D, axisymmetric 8-nodes element is generated to simulate the cylinder clay soil sample, as illustrated in Fig. 2(a). In computation, the bottom of axisymmetric element is fixed in vertical; and the axisymmetric line is fixed in horizontal. The confining pressure σ'_3 , and axial pressure σ'_1 applied on the cylinder soil sample are varied according to the expected stress path. There are totally two stress paths, OA and OB respectively, in this verification work, as shown in Fig. 2(b). Before applying axial deviatoric stress in vertical, soil sample is firstly isotropically consolidated at $p_0=196$ kPa. After fully consolidated, the soil sample is sheared according to the expected stress path OA and OB, in which OB is a conventional drained path, while OA is a constant confining pressure path. The axial strain ϵ_1 , radial strain ϵ_r , volumetric stress ϵ_v are recorded in computation.

The comparison between the test results and that predicted by FSSI-CAS 2D for the normally consolidation Fujinomori clay adopting modified Cambridge soil model are demonstrated in Fig. 3. It is observed that the results predicted by FSSI-CAS 2D agree very well with the test results provided by Nakai and Matsuoka (1986), indicating that FSSI-CAS 2D can highly reliably describe the mechanical behavior of clay soil. This verification is a solid foundation for the subsequent numerical analysis in the study.

4. Engineering background

Yantai port is located on the southwest coastal line of Bohai Bay, and is geographically affiliated to the city of Yantai, Shandong Province, China, as illustrated in Fig. 4. Currently, Yantai port includes

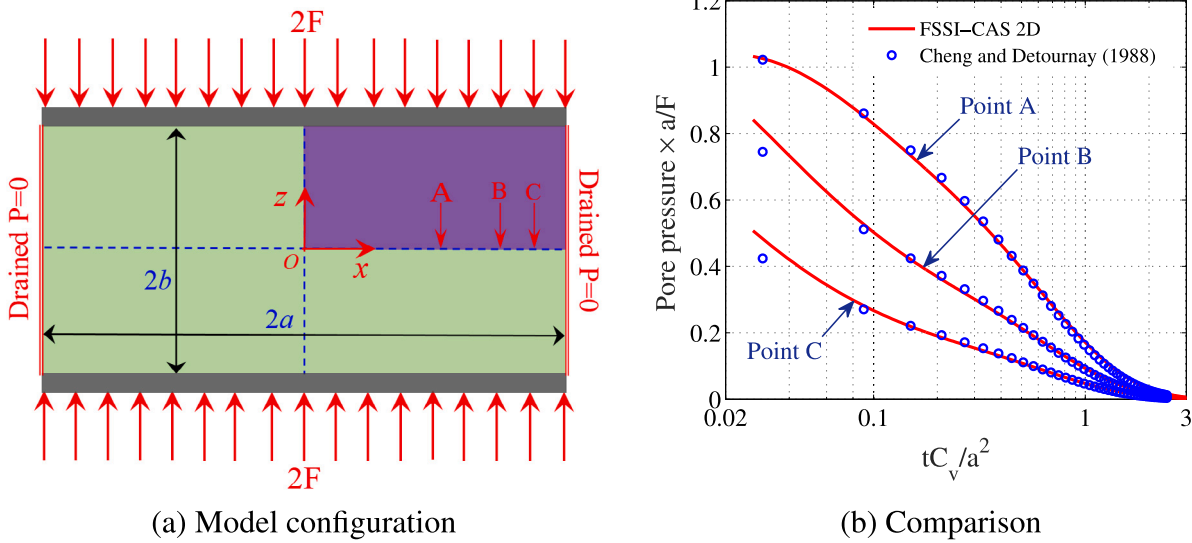


Fig. 1. Comparison of the pore pressure dissipation between the present model's result and the analytical solution (Noted: A ($x = \frac{a}{2}, z = 0$), B ($x = \frac{3a}{4}, z = 0$) and C ($x = \frac{7a}{8}, z = 0$)).

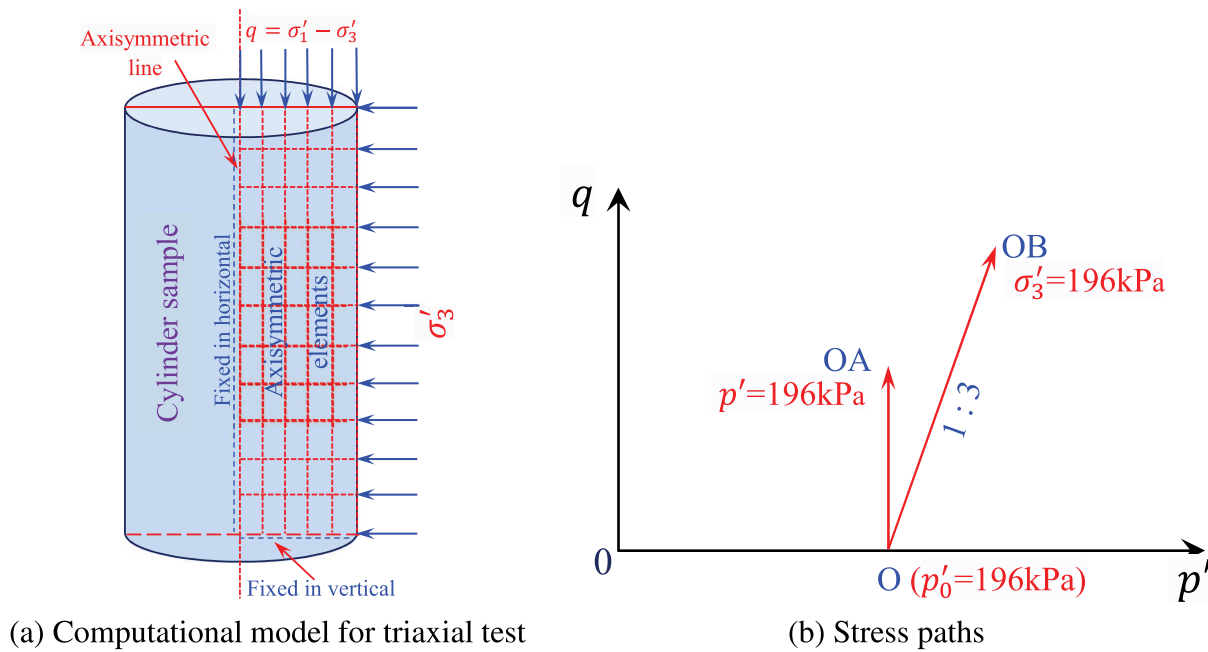
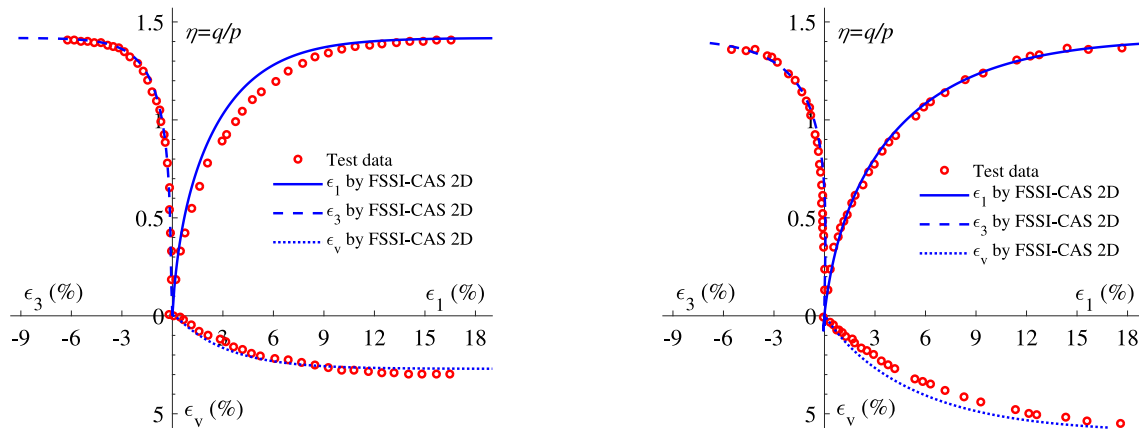


Fig. 2. Schematic map of the computational model for the triaxial test of clay soil and the two typical stress paths.

four harbour zones. They are chifu bay zone, west harbour zone, longkou harbour zone and penglai harbour zone, respectively. Among them, the west harbour zone is the largest one; and is the core asset for the development of Yantai port. Total length of the wharfs in the west harbour zone is 19 km. The maximum water depth in front of the wharfs is 28 m. The west harbour zone is divided into 8 functional zones such as container, chemical liquid, bulk cargo, general bulk, crude oil and LNG etc. Totally, 65 berths with the capacity 50,000 to 300,000 tons will be constructed. The planned ultimate bearing capacities of the west harbour zone will be up to 200 million tonnes and 15 million standard containers per year.

In order to guarantee the safety of vessels when docking in front of the wharfs for loading and unloading, a group of deep water breakwaters have been constructed to surround a harbour basin with a area about 5 km², as illustrated in Fig. 5. In the west harbour zone, the whole breakwater construction project is divided into two phases.

The structure form of phase I is the sloping rubble mound breakwater covered by accropodes, as shown in Fig. 6; and it is composite breakwater in phase II. Currently, the construction of breakwaters in phase I and phase II have all been finished. The stability of the composite breakwaters in phase II under extreme fortified ocean waves impact has been evaluated by He et al. (2018). As shown in Fig. 6, the width at the bottom and at the top of the rubble mound breakwater (referred as RB breakwater thereafter) is up to 130 m, 15.52 m, respectively; meanwhile, the height is up to 23 m. It is known that this rubble mound breakwater is large in size, resulting in that a great weight will be applied to its underlying seabed foundation. According to the collected geological profiles in the geotechnical surveying stage, the underlying seabed foundation mainly consist of muddy-silty clay, silty clay, clay and silty soils. Significant compressive deformation would occurred in the seabed foundation due to the low bearing capacity of these foundation soils, and would further result in the excessive subsidence



(a) Stress path OA

(b) Stress path OB

Fig. 3. Comparison between the test results and that predicted by FSSI-CAS 2D for the Fujinomori clay adopting modified Cambridge soil model.



Fig. 4. Position of Yantai port locating at (E121.3537, N37.6183).

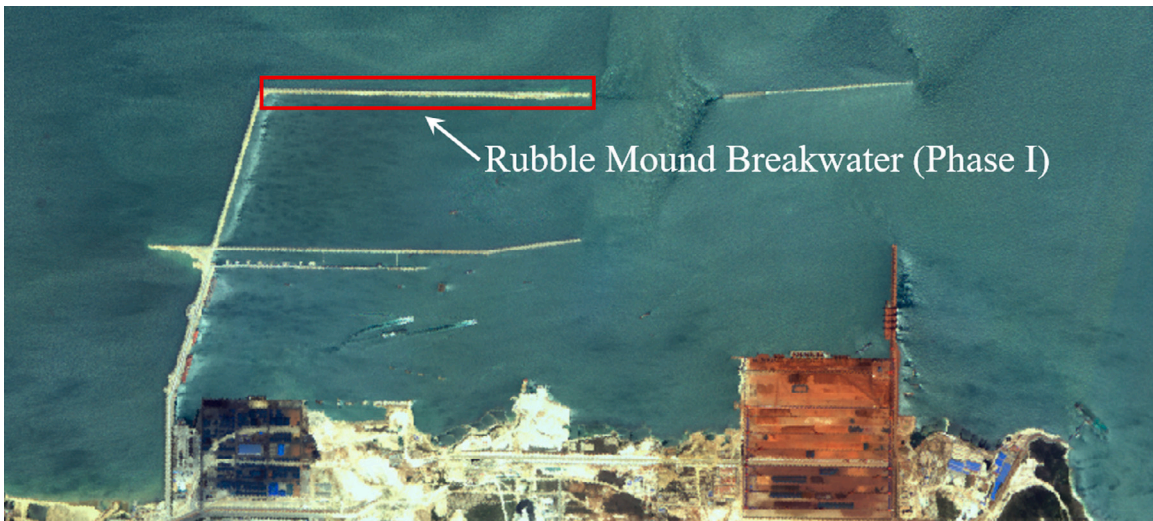


Fig. 5. Satellite top view of the west harbour zone of Yantai port.

of the overlying rubble mound breakwater after construction. In order to provide some reserved height for the rubble mound breakwater in design stage, making the top elevation of the rubble mound breakwater approach to the designed elevation after subsiding finished, it is highly necessary to predict the subsidence of the large-scale rubble mound

breakwater built on the seabed foundation with low bearing capacity in the west harbour zone of Yantai port.

In this study, taking the rubble mound breakwaters constructed in phase I at the west harbour zone as the representative, the developed numerical model FSSI-CAS 2D is adopted to predict the subsidence

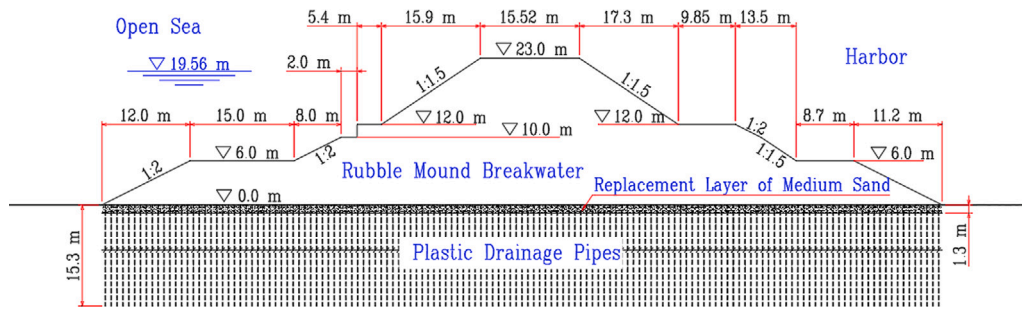


Fig. 6. Computational domain and dimensions of the rubble mound breakwater at the west harbour zone of Yantai port.

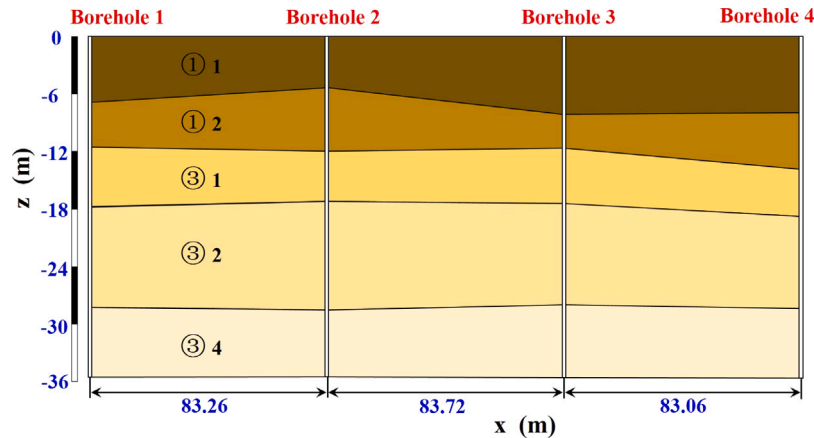


Fig. 7. Profiles of seabed foundation soil layers coming from field boreholes survey. ①₁: muddy-silt clay, ①₂: Silty Clay, ③₁: Clay, ③₂: Silty Clay and ③₄: Silt.

Table 2
Basic physical properties of seabed foundation soil layers.

Stratum	w (%)	γ (kN/m ³)	e	W _L (%)	I _p (%)	I _L	ϕ' (°)	c' (kPa)
Muddy-silty Clay ① ₁	39.6	17.9	1.08	32.1	14.5	1.52	18.1	15
Silty Clay ① ₂	32.3	18.5	0.91	29.3	13.1	1.24	19.9	20
Clay ③ ₁	27.5	19.5	0.77	42.8	21.3	0.28	23.4	35
Silty Clay ③ ₂	23.4	20.0	0.64	28.2	12.8	0.63	27.1	26
Silt ③ ₄	22.3	19.9	0.62	24.7	7.4	0.66	25.5	38
Stratum	a _{0.1-0.2} (MPa)	E _{50.1-0.2} (MPa)	C _c	SPT (N)	f (kPa)	k (cm/s)	C _{vV} (cm ² /s)	C _{vH} (m ² /s)
Muddy-silty Clay ① ₁	0.73	2.92	0.26	1.0	70	3.7e-7	1.72	2.35
Silty Clay ① ₂	0.52	3.94	0.21	2.0	90	2.6e-7	4.12	4.80
Clay ③ ₁	0.28	6.66	0.23	15.0	180	9.6e-6	1.00	0.95
Silty Clay ③ ₂	0.26	6.76	0.15	13.0	180	4.0e-6	4.33	4.05
Silt ③ ₄	0.18	9.42	0.11	28.0	200	5.8e-6	8.54	8.13

of the breakwaters, to provide engineers with the settlement value, making the reserved redundant height of the rubble mound breakwater more appropriate in design stage. To implement this application, the profiles and basic physical properties of the seabed soil layers, which is as the foundation of the RB breakwaters at the west harbour zone, were firstly collected from the consultant company in charge of the in-situ geotechnical survey in the west port zone. As demonstrated in Fig. 7, there are mainly five soil layers in the seabed foundation of the RB breakwaters. They are muddy-silt clay ①₁, Silty Clay ①₂, Clay ③₁, Silty Clay ③₂ and Silt ③₄, respectively. Their basic physical properties of the five seabed soil layers obtained by performing a series of geotechnical tests are listed in Table 2. It can be seen that the muddy-silt clay ①₁ and ①₂ are weak soil layers with a thickness of 12 m to 14 m. Their water content is up to 39.6% and 32.3%; void ratio is around 1.0; and the bearing capacity f is only 70, 90 kPa, respectively. In engineering practice, the surface layer with a thickness of 1.3 m of the first soil layer ①₁ exactly beneath the rubble mound breakwater was replaced with dense medium sand to enhance the bearing capacity of the seabed

foundation. Furthermore, a great number of plastic drainage strips with a length of 14 m were inserted into the soil layers ①₁ and ①₂ with a spacing of 1.0 m, to improve their seepage permeability, as illustrated in Fig. 6. This engineering measure can effectively to accelerate the process of consolidation of the seabed foundation, as well as reduce the subsiding of overlying rubble mound breakwaters to some extent. In Table 2, it is also can be found that the seabed soil layers ③₁, ③₂, ③₃ all have relatively excellent bearing performance with their bearing capacity is in the range of 180 kPa to 200 kPa.

5. Computational domain, boundary condition and soil parameters

According to the design diagram of the rubble mound breakwater in the west harbour zone of Yantai port, as shown in Fig. 6, and the profiles of seabed soil layers in Fig. 7, the computational domain used in this study to predict the subsidence of the rubble mound breakwater

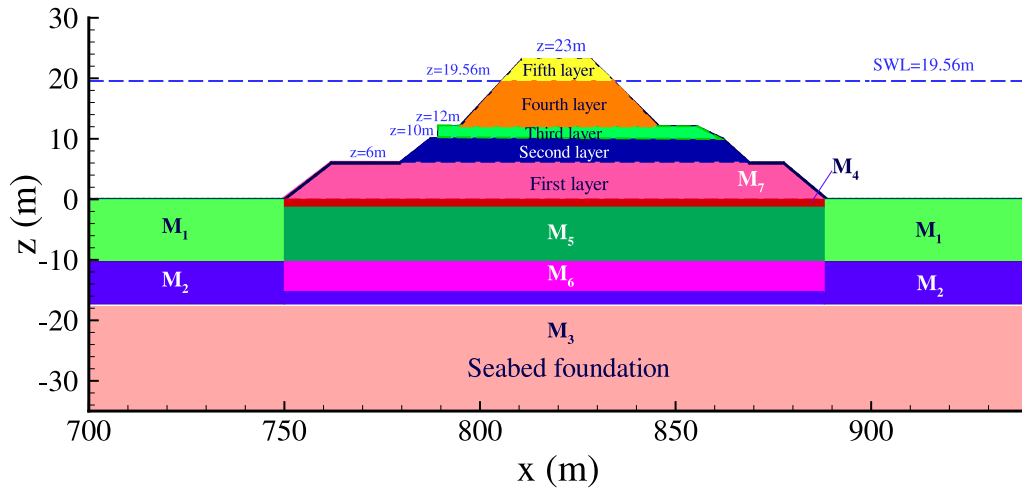


Fig. 8. Material zones for the mesh generation in computation.

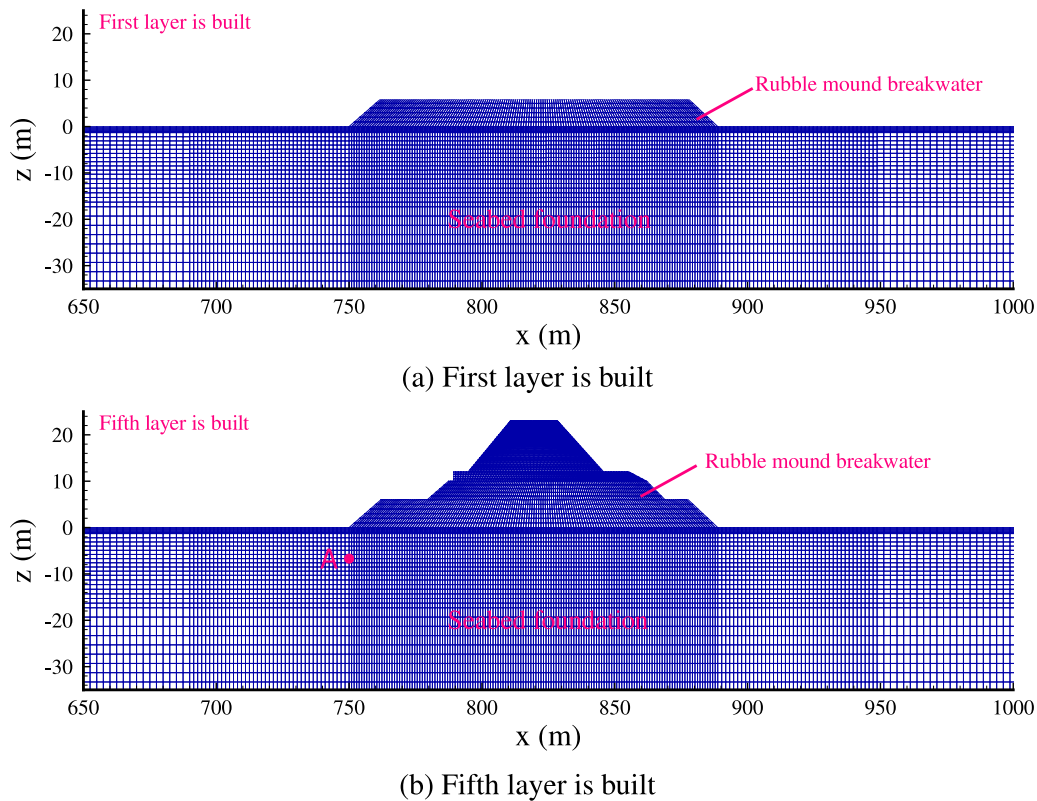


Fig. 9. The generated mesh in the computational domain after the first and fifth layer of the rubble mound breakwater is built (Noted: A ($x=750$ m, $z=-6.7$ m) is a typical position under the RB breakwater selected as the representative for time history analysis).

in the west harbour zone of Yantai port is illustrated in Fig. 8. The total length of the computational domain is 750 m ($x=350$ m to $x=1100$ m). The width at bottom of the rubble mound breakwater is 130 m. Its distance to the left and right boundary of the seabed foundation is 400 m and 210 m, respectively. Due to the fact the maximum depth of surveying boreholes in the seabed floor on which this rubble mound breakwater is built is only 35.5 m, the thickness of the seabed foundation in the computation is set as 35.5 m, correspondingly. In this study, the seabed surface is set as $z=0$ m; and the left side of the seabed foundation is set as $x=350$ m. Besides, the SPT of $\textcircled{3}_4$ is 28, and its bearing capacity is 200 kPa as that listed in Table 2. It means the soil layer $\textcircled{3}_4$ is very hard. Therefore, taking the soil layer $\textcircled{3}_4$ as the bottom of computational domain has the reasonability.

In computation, the following boundary conditions are applied:

(1) The lateral sides of seabed foundation are fixed in horizontal.

$$u_s|_{left\ side} = u_s|_{right\ side} = 0 \quad (7)$$

(2) The bottom of seabed foundation is fixed in both horizontal and vertical, and treated as a impermeable board.

$$u_s = w_s = 0 \quad \text{and} \quad \frac{\partial p}{\partial z} = 0 \quad \text{at} \quad z = -35.5\text{m} \quad (8)$$

(3) On the surface of the seabed floor and the outer surfaces of the rubble mound breakwater, the total hydrostatic pressure is applied. According to the hydrological survey, the average water depth in front of the rubble mound breakwater is 19.56 m under the condition of

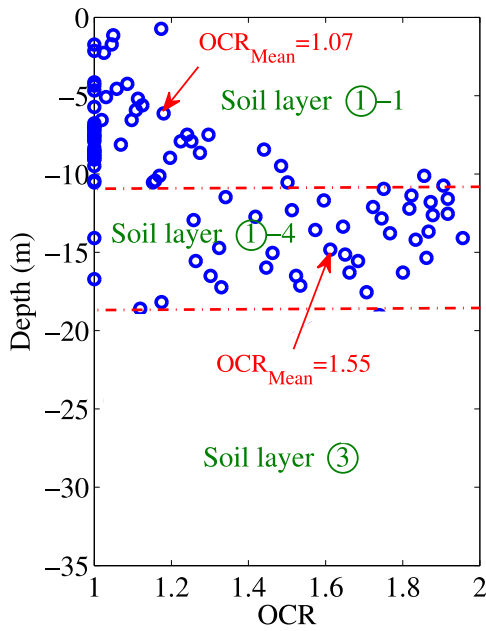


Fig. 10. Distribution of the measured OCR along the depth of seabed foundation.

normal sea state. Therefore, the hydrostatic water pressure can be determined following $p = \rho \times (19.56 - z)$, and its applying direction is perpendicular to the surface of the rubble mound breakwater and its seabed foundation. This application of the hydrostatic water pressure makes the buoyancy applied on these rubble mounds can be considered in computation. As we known, there must be buoyancy for these rubble mounds under SWL due to the fact that some water has been expelled by them. As a result, the pressure on the bottom of structure induced by the overlying rubble mound breakwater is much less than if the buoyancy is not taken into consideration. Therefore, the hydrostatic water pressure must be applied. Otherwise, the subsidence of structure will be overestimated due to the overestimation of the bottom pressure of structure. Additionally, it is worth to point out that the hydrostatic pressure at a position is not a constant, but would be changed accompanying the subsiding of structure and the deformation of seabed foundation, especially in the cases large deformation or/and great subsidence are involved. Fortunately, FSSI-CAS 2D can timely update the hydrostatic pressure on boundary nodes by checking the current position of each boundary nodes at each time step in computation. This variation of hydrostatic pressure on boundaries can be effectively handled by FSSI-CAS 2D. This is one of the priorities of FSSI-CAS 2D in solving the nonlinear interacting between seawater, structure and its seabed foundation under dynamic or quasi-static loading.

(4) Finally, the effective stress component perpendicular to the outer surface of structure and its seabed foundation, as well as the shear stress on it must be kept as zero all the time in computation, due to the

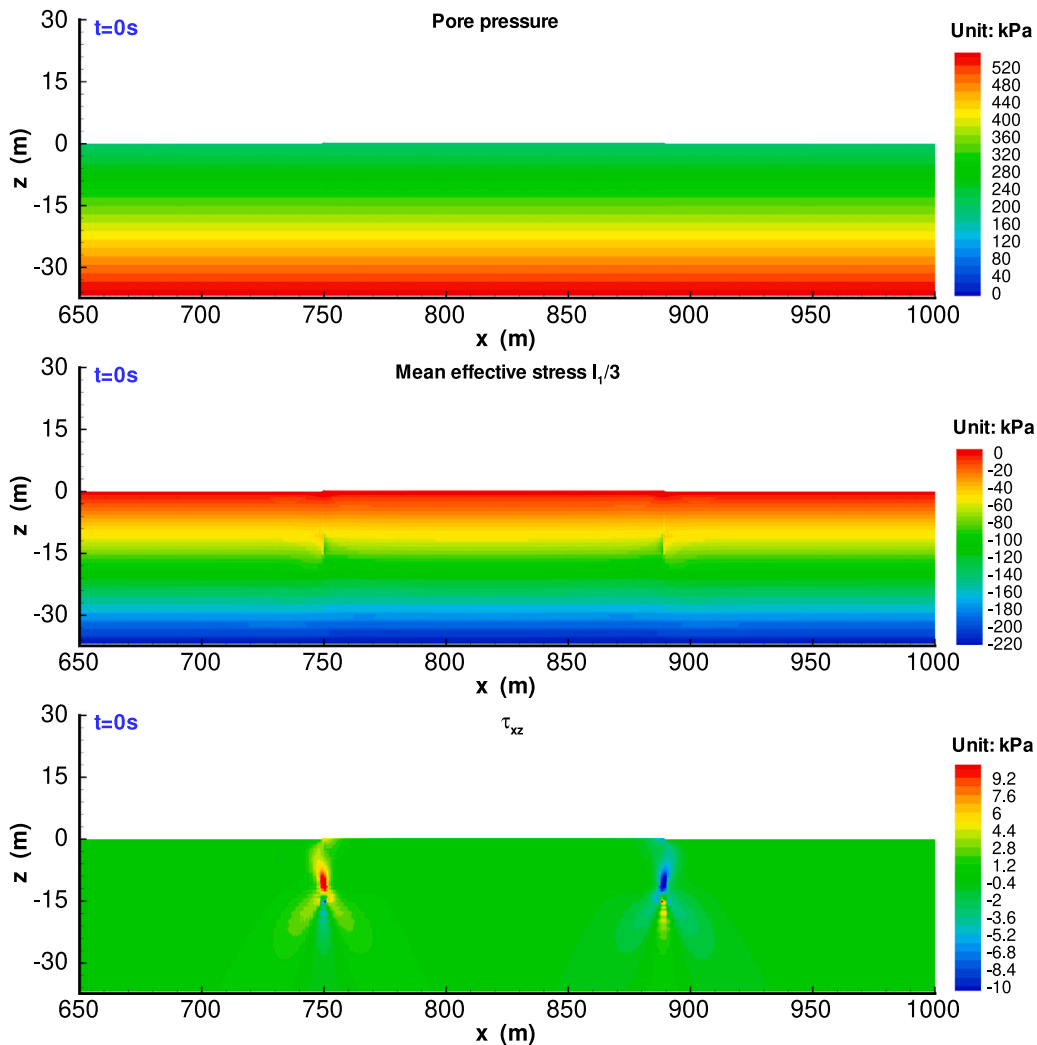


Fig. 11. Distribution of pore pressure, effective stress in the seabed foundation at the initial state.

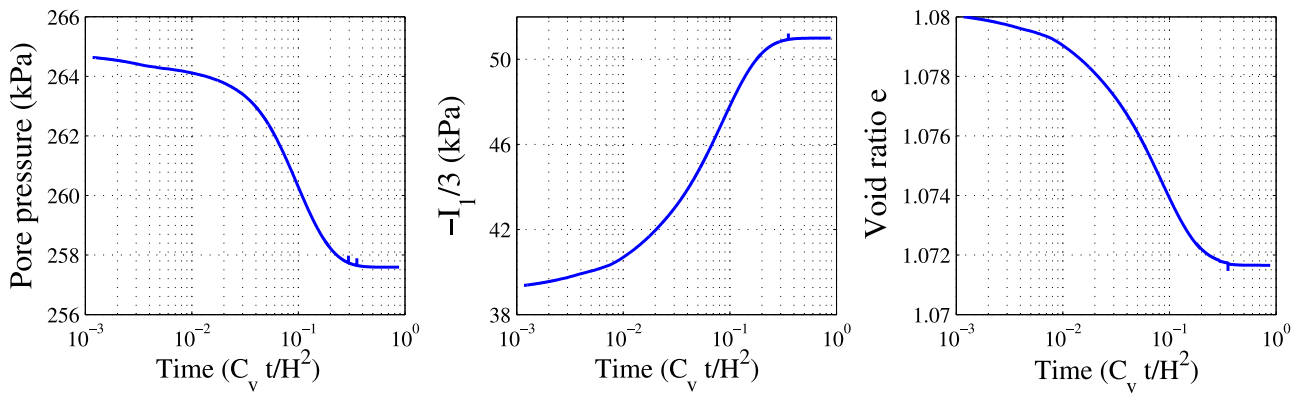


Fig. 12. Process of pore pressure dissipation, mean effective stress increase and void ratio reduction at the typical position A ($x=750$ m, $z=-6.7$ m) after the first layer is built (Noted: H is the thickness of seabed foundation).

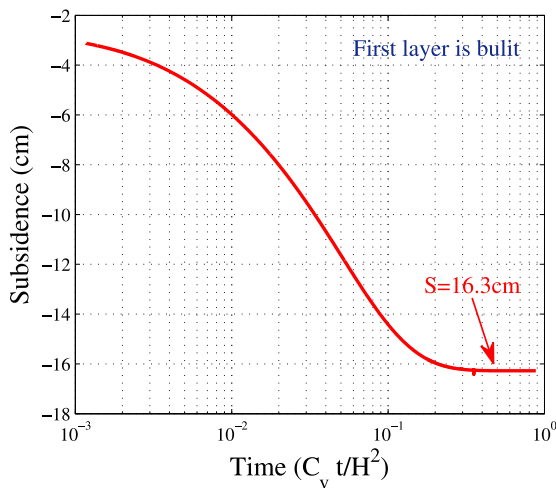


Fig. 13. Process of the subsidence of the rubble mound breakwater after the first layer is built.

fact that the rubble mound breakwater and its seabed foundation are both porous medium, rather than impermeable structure or medium. Otherwise, the stress boundary condition on the outer surface of the rubble mound breakwater and the seabed foundation is wrong.

As demonstrated in Fig. 7, there are totally seven types of material in the computational domain. The seabed foundation is divided into three material zones. They are M1 ($z = -10$ to 0 m) for the soil layer ①₁ and ①₂ due to their similar properties; M2 ($z = -17$ to -10 m) for the soil layer ③₄, and M3 ($z = -35.5$ to -17 m) for the soil layer ③₂ and ③₄ due to their similar properties as illustrated in Table 2. The replacement layer with a thickness of 1.3 m beneath the rubble mound breakwater is set as material M4. As stated above, a great number plastic drainage trip have been inserted into the materials M1 and M2 to enhance the vertical permeability of the soil layers. The soil in which the plastic drainage strips are inserted in the soil layer ①₁ and ③₁ is set as material M5, M6 respectively. The rubble mound breakwater is set as material M7, and is divided into fine layer based on the characteristics of its outer shape. In FE computation, the weight of these rubble mounds (buoyancy is considered under SWL=19.26) is applied in the way of layer by layer.

In this study, the modified Cambridge clay soil model is adopted to describe the mechanical behavior of the material M1, M2, M5, M6 due to the fact that M1, M2, M5 and M6 have significant compressibility caused by their relatively low bearing capacity. The rubble mound breakwater M7 is described adopting poro-elastic soil model because these rubble mounds mixture are very strong relative to soil. M4 is a

kind of dense medium sand to replace the muddy-clay in engineering. Therefore, pore-elastic soil model is also used for M4. Due to the fact that the material M3 for the soil layers ③₂ and ③₄ has a great bearing capacity ($f=180-200$ kPa) and high value of SPT (13 to 28), it means the soil layer ③₂ and ③₄ will contribute little to the subsidence of the overlying structure. Based on this recognition, pore-elastic soil model is also used for material M3. In computation, the mesh is generated according to the loading applying process of the overlying rubble mound breakwater in the way of layer by layer, as shown in Fig. 9. Once one layer of rubble mounds is built, the subsidence of the breakwater is predicted until to its stable state. After that, the next layer of rubble mounds is built in the mesh system and the subsidence is continuously predicted by FSSI-CAS 2D until the fifth layer is built. Finally, the subsidence of the rubble mound breakwater could be totally predicted.

It is an indisputable fact in the field of geomechanics that the reliability of the computation results is highly dependent on the accuracy of soil/rock's physical parameters. In this study, the modified Cambridge clay model (referred as MCC model thereafter) and poro-elastic model are used to describe the quasi-static mechanical behavior of the seabed foundation soil. Therefore, it is necessary to determine the model parameters needed by the modified Cambridge clay and pore-elastic model for the seven types of material M1 to M7. Actually, a number of conventional laboratory and in-site geotechnical testing work in the field surveying stage have been conducted by engineers according to the Chinese Code for Investigation of Geotechnical Engineering of ports (JTS-133-1-2010), and the Code of Design and Construction of Breakwater (JTS-154-1-2011). All the physical properties of the five soil layers measured in these tests have been listed in Table 2. However, the model parameters of the five soil layers for the modified Cambridge clay or pore-elastic model were not given by engineers involved in the laboratory testing. As a result, the model parameters of M1 to M7 for the MCC or pore-elastic model have to be estimated according to the property parameters listed in Table 2.

In the MCC model, there are five model parameters needed in computation. They are Poisson's ratio ν , other slope of critical state line (CSL) M_f in p - q coordinates, the slope of Normal Consolidation Line (NCL) λ in e - $\ln p$ coordinates and the slope of the rebounding Line in e - $\ln p$ coordinates and finally the overconsolidation ratio (OCR) of soil at a position. Firstly, M_f can be estimated as following

$$M_f = \frac{6 \sin(\phi)}{3 - \sin(\phi)} \quad (9)$$

where ϕ is the friction angle of soil. ϕ and ν both can be measured in conventional drained triaxial test. Secondly, λ can be estimated adopting the formulation $\lambda = \frac{C_c}{2.3}$. Where C_c is the compression index. The value C_c of the five soil layers have been given in Table 2. Generally, κ is 1/2-1/5 of λ depending on the strength of soils. For soft soil, κ generally is much less than λ . In this study, κ is set as 1/3 of λ for M1, M4 and is set as 1/4 of λ for M2, M5. Fortunately, the

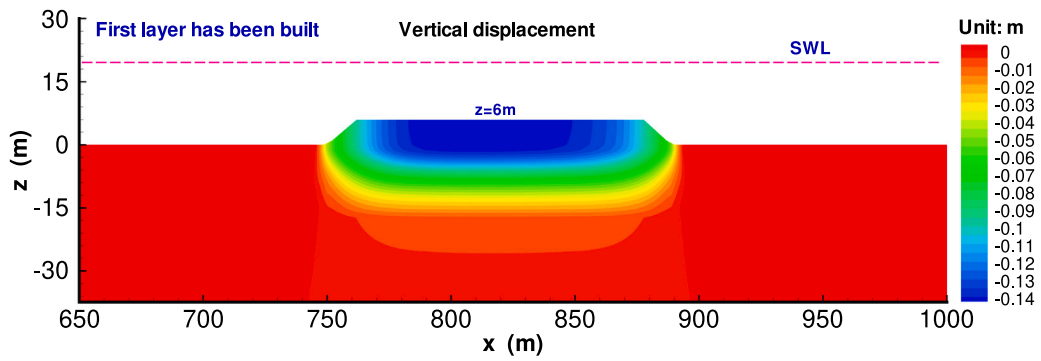


Fig. 14. Distribution of the vertical subsidence after the first layer is built.

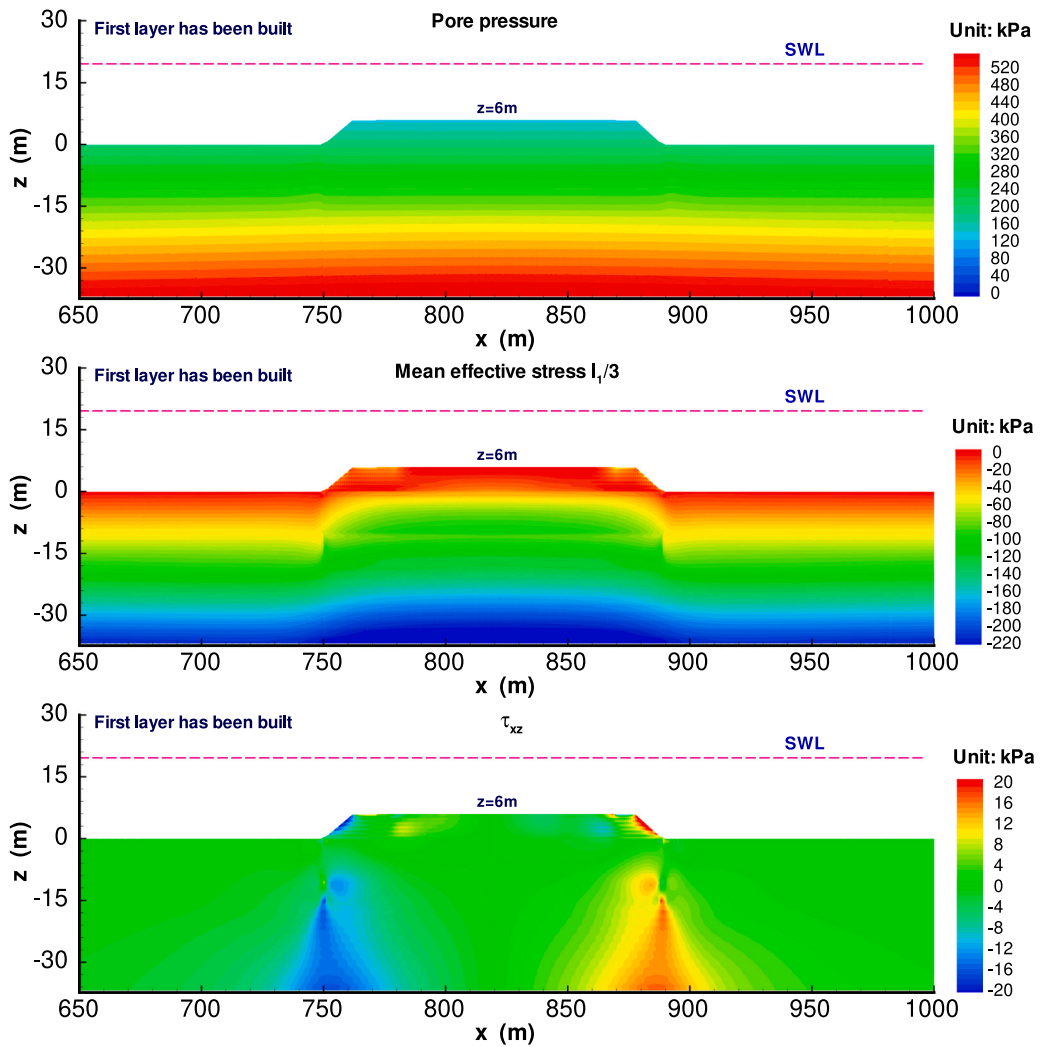


Fig. 15. Distribution of pore pressure, effective stress in the seabed foundation after the first layer is built.

value of OCR has been measured in the geotechnical surveying stage. The distribution of OCR along the depth is demonstrated in Fig. 10. It is observed that the distribution of OCR in the seabed foundation in the soil layer ①₁, and ①₄ is not concentrated, but scattered. However, the OCR in the soil layer ①₁ overall is less than that in the soil layer ①₄. The mean value of the measured OCR is 1.07 in the soil layer ①₁, and is 1.55 in the soil layer ①₄. Therefore, the OCR is set as 1.07 for M1, M5, 1.55 for M2, M6.

For the material M3, Young's modulus E and Poisson's ratio ν is needed by the pore-elastic model. The E of M3 can be estimated

according to

$$E = \frac{(1 + \nu)(1 - 2\nu)}{(1 - \nu)} E_s \quad (10)$$

where E_s is the deformation modulus, which has been given out in Table 2. ν is set as 0.3 for M3 in computation, and 0.38 for M1, M2, M5, M6. M4 is dense medium sand, its E is set as 100MPa, $\nu=0.35$. Material M7 is composed of large rubble mounds. Its E is set as 10 GPa, $\nu=0.25$. Finally, all the model parameter and properties of M1 to M7 are listed in Table 3. It must be pointed out that the permeability of foundation

Table 3
Model parameters of the seabed foundation soil layers for the modified Cambridge clay model and poro-elastic model.

	Material	M1	M2	M3	M4	M5	M6	M7-M10
Poro-elastic	E	–	–	80 (MPa)	30 (MPa)	–	–	200 (MPa)
	ν	–	–	0.28	0.25	–	–	0.25
Modified Cambridge clay model	M_f	0.772	1.07	–	–	0.772	1.07	–
	λ	0.113	0.0696	–	–	0.113	0.0696	–
	κ	0.0283	0.0348	–	–	0.0283	0.0348	–
	ν	0.35	0.3	–	–	0.35	0.3	–
	OCR	1.07	1.55	–	–	1.07	1.55	–
Basic properties	e	1.08	0.62	0.50	0.60	1.08	0.62	0.60
	S_r	99%	99.3%	99.5%	99.1%	99.1%	99%	100%
	k_x ($\mu\text{m/s}$)	0.85	35	50	1000	10	10	1.0×10^4
	k_z ($\mu\text{m/s}$)	0.3	20	30	2000	20	0.85	1.0×10^4

soils basically has no effect on the final magnitude of subsidence, but the speed of consolidation process will be significantly affected by the permeability of soil layer.

6. Results

6.1. Initial status

Before the rubble mound breakwater is built, there is an initial state of effective stress, pore pressure and displacement in the seabed foundation. This initial state must be determined first for the thereafter structures subsidence computation, because the current stress state must be known in advance to judge the current overconsolidation state of soil, through comparing the current stress with the greatest stress in history if the modified Cambridge clay model is used. It is known that the vertical displacement in the seabed foundation must be very small due to the fact that there is no external loading applied on the seabed floor before the overlying offshore structure is constructed. However, this initial displacement has to be set as 0 in the thereafter subsidence analysis, because this initial state is a natural state, which has been occurred in the past geological history. This natural initial vertical displacement will certainly not cause the subsidence of overlying structures.

The distribution of the pore pressure, and effective stress in the seabed foundation before the rubble mound breakwater is constructed are illustrated in Fig. 11. It is found that the initial pore pressure and $I_1/3$ is distributed in layers. There is no any excess pore pressure in the seabed foundation before the rubble mound breakwater is constructed. It is interesting to observe that there are two concentrated zone of shear stress along the two interfaces between M1, M2 and M5, M6. This phenomenon is mainly attributed to that the stiffness of material M1, M2 and M5, M6 are significantly different. If the physical properties of M1, M2, M5 and M6 are the same. Then this shear stress concentrated zone will disappear.

6.2. Subsidence after first layer is built

Taking the initial stress and pore pressure as the initial condition ($t=0$), the subsidence process after the first layer rubble mounds is built can be numerically predicted adopting FSSI-CAS 2D. Fig. 12 demonstrates the variation process of the pore pressure p , mean effective stress $I_1/3$ and void ratio at the type position A ($x = 750$ m, $z = -6.7$ m) in the subsiding process of the rubble mound breakwater after the first layer is built. It is observed that the pore pressure in the seabed foundation beneath the breakwater has significantly increased at the initial early stage, because the loading induced by the weight of the first layer is totally undertaken only by the pore water in the seabed soil beneath the breakwater. After that, the pore pressure in the seabed foundation gradually dissipates until to its initial hydrostatic value, accompanying the pore water is drained out of the seabed which is driven by pore pressure gradient. In this process, the loading undertaken by the pore water gradually is transmitted to the soil particles of seabed, making the

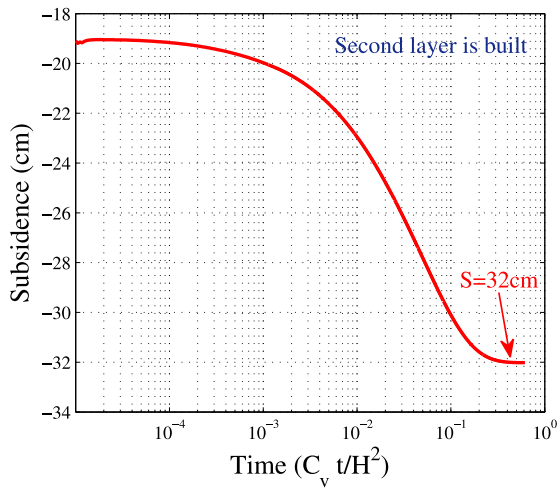
mean effective stress in the seabed foundation gradually increase until to reach its stable state. Meanwhile, the increasing of the mean effective stress further cause the seabed foundation soil being compressed, resulting in the void ratio of the seabed soil gradually reducing, as illustrated in Fig. 12. As a result, the overlying rubble mound breakwater gradually subsidence correspondingly, as that demonstrated in Fig. 13. It is shown that the subsidence of the first layer after it is built is 16.3 cm.

The distribution of the vertical subsidence after the first layer is built are shown in Fig. 14. It is observed that the subsidence of first layer is not uniform. The subsidence of the central zone in the first layer is much greater than that in the two lateral zones. And only the seabed soil beneath the rubble mound breakwater is compressed. There is basically no subsidence in the seabed foundation away from the RB breakwater due to the fact that there is no external loading is applied on it. The distribution of pore pressure, mean effective stress $I_1/3$ and shear stress τ_{xz} when the consolidation process has finished after the first layer is built is demonstrated in Fig. 15. The mean effective stress $I_1/3$ in the zone beneath the RB breakwater has significantly increased due to the fact that the weight of the first layer rubble mounds has been completely undertaken by beneath seabed foundation when the consolidation process has finished. It is also found that there are two shear stress concentrated zones in the seabed foundation under the two lateral parts of the RB breakwater. The maximum magnitude of τ_{xz} could be greater than 20 kPa.

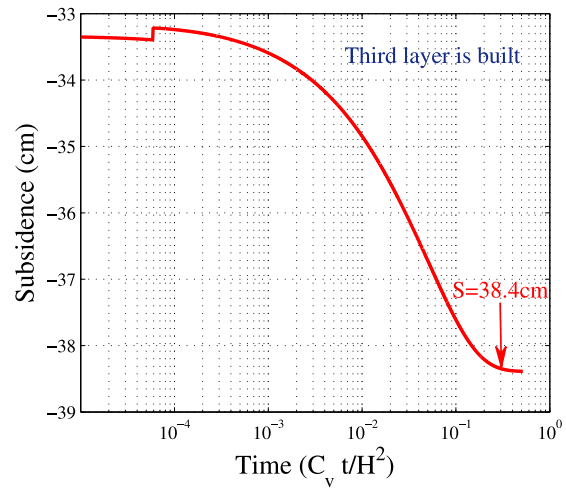
6.3. Subsidence after second to fifth layer is built

For the sake of simplicity, the consolidation and subsidence process of the RB breakwater after the second layer to fifth layer is respectively built are discussed and analyzed together in this section. The subsiding processes of the RM breakwater after the second layer to fifth layer is respectively built are demonstrated in Fig. 16. It is found the subsiding process shown in Fig. 16 are basically the same with that after the first layer is built. The only difference is that the subsidence of the RM breakwater becoming greater and greater after the rubble mounds breakwater is built in the way of layer by layer. In Fig. 16(d), it is known that the final subsidence of the RM breakwater is predicted as 64.1 cm by the numerical model FSSI-CAS 2D after the total five layers of rubble mounds are all constructed. This magnitude of post-construction subsidence is considerable. A redundant height with about 0.7 m should be reserved in design for the purpose that the top elevation of the RB breakwater could reach the designed requirement. Otherwise, the RB breakwater maybe cannot normally service after its subsidence is finished.

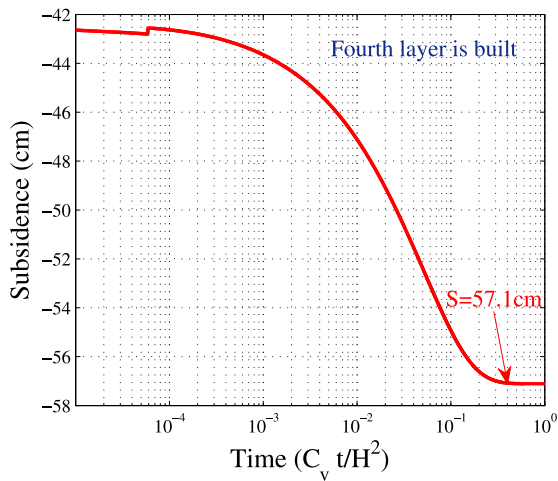
Except the time history of the subsiding, the distributions of the vertical subsidence of the RM breakwater and its seabed foundation after the second layer to fifth layer is respectively built are illustrated in Fig. 17. In Fig. 17, it is observed that the distribution characteristics of the subsiding in the RM breakwater and its foundation is basically similar with that after the first layer is built. The subsidence of the middle part of the RM breakwater is significantly greater than that of the lateral parts, and only the seabed soil beneath the RM breakwater



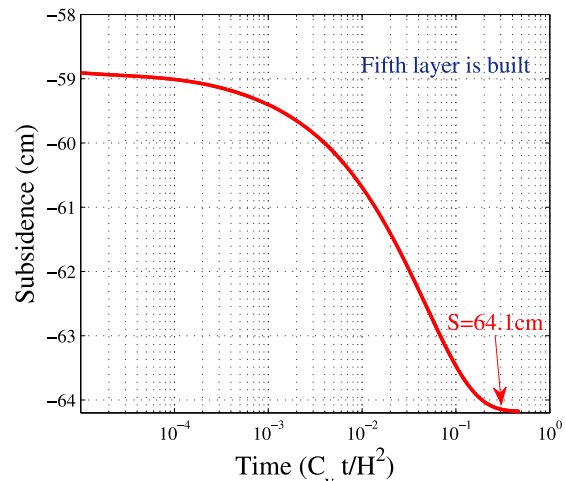
(a) Second layer is built



(b) Third layer is built



(c) Fourth layer is built



(d) Fifth layer is built

Fig. 16. Process of the subsidence of the rubble mound breakwater after the second to fifth layer is respectively built.

is compressed. There is basically no the vertical subsidence in the seabed foundation zone away from the RM breakwater. Accompanying the construction process of the rubble mounds layer by layer, the magnitude of the subsidence of the RM breakwater gradually increases. However, it is worth to point out that the variation process of the pore pressure, mean effective stress and the void ratio in the seabed foundation is not ways monotonically increased or reduced, as that shown in Fig. 12. Fig. 18 illustrates the process of the pore pressure, mean effective stress and the void ratio at the typical position A after the fourth layer is built. As demonstrated in Fig. 18, the pore pressure is increased, $I_1/3$ is reduced before the time $c_v t/H^2 = 0.06$. Meanwhile, the seabed soil at position A is dilated. After the time $c_v t/H^2 = 0.06$, the pore pressure gradually dissipate, and the mean effective stress increases correspondingly. Meanwhile, the seabed soil at the position A is gradually compressed accompanying the pore water is drained out, until to the stable state. This non-monotonic variation process of pore pressure and effective stress is a typical Mandel–Cryer effect. It is indicated that the subsiding of the RM breakwater and consolidation of seabed foundation is a complicated nonlinear process.

The distributions of the final pore pressure, mean effective stress and shear stress after the RM breakwater is completely constructed are illustrated in Fig. 19. It is observed that the pore pressure is also distributed in layers. There are will no excess pore pressure in

the seabed foundation because it has been completely dissipated. The effective stress in the foundation beneath the RM breakwater has significantly increased due to the gravity compression of the overlying RM breakwater. There are still two shear stress concentrated zones in the seabed foundation under the two lateral parts of the RM breakwater, and the area of the concentrated zones are much larger in size than that after the first layer is built. It is also found that there are also two shear stress concentrated zones in the two lateral slopes in the RM breakwater. The maximum magnitude of the concentrated shear stress reaches up to 70–80 kPa in the two lateral slopes. This magnitude is much greater than that in the beneath seabed foundation. Due to the fact that the strength resisting shearing of the rubble mound layers is much greater than the maximum shear stress generated in the lateral slopes, the stability against slope sliding of the RM breakwater can be guaranteed.

6.4. Comparison with observation data

In the practice of engineering, the whole RM breakwater was constructed one section by one section, and was constructed layer by layer in one section. A number of displacement sensors have been installed on the rubble mound breakwater at different typical cross sections once they were successfully constructed.

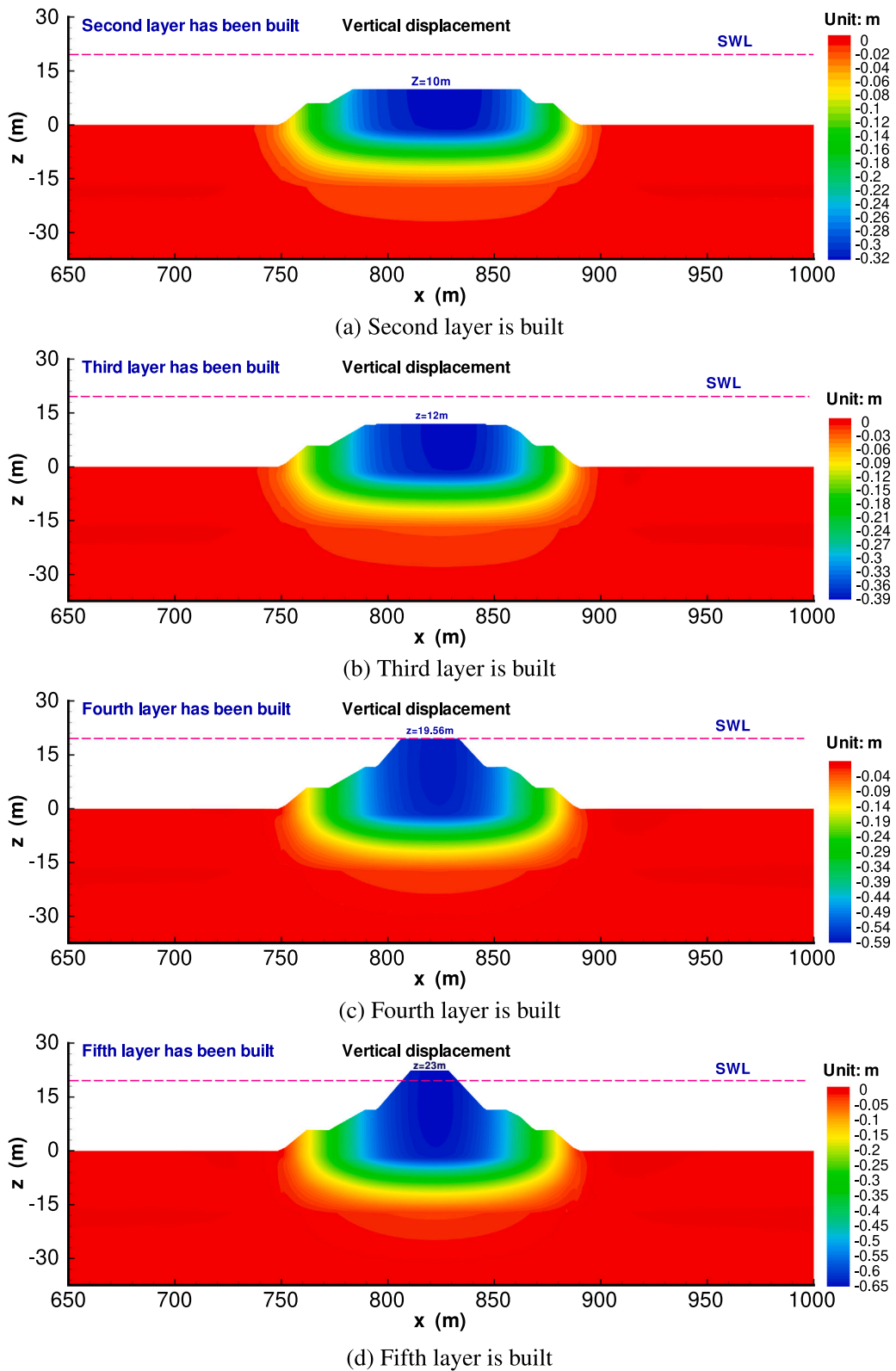


Fig. 17. Distribution of the vertical subsidence after the second to fifth layer is respectively built.

The time history of the subsidence recorded by these sensors (NO. 1 to NO. 18) are shown in Fig. 20. It is known that the starting date to record the subsidence of the RM breakwater is different from different sensors. The earliest date starting to monitor is 15th May 2013 (NO.1), and the latest date is 18th October 2013 (No.18). Correspondingly the longest period for the monitoring is 192 days, and shortest period is

only 60 days. Due to the fact that the longer the monitoring period, the more reliable the monitoring data for the subsidence of structures, only the monitoring data recorded for more than 100 days as shown in Fig. 20(a) are adopted to verify the numerical result predicted by FSSI-CAS 2D. In Fig. 20(a), it is known that the subsidence of the rubble mound breakwater is in the range of 44 cm to 76 cm. Meanwhile,

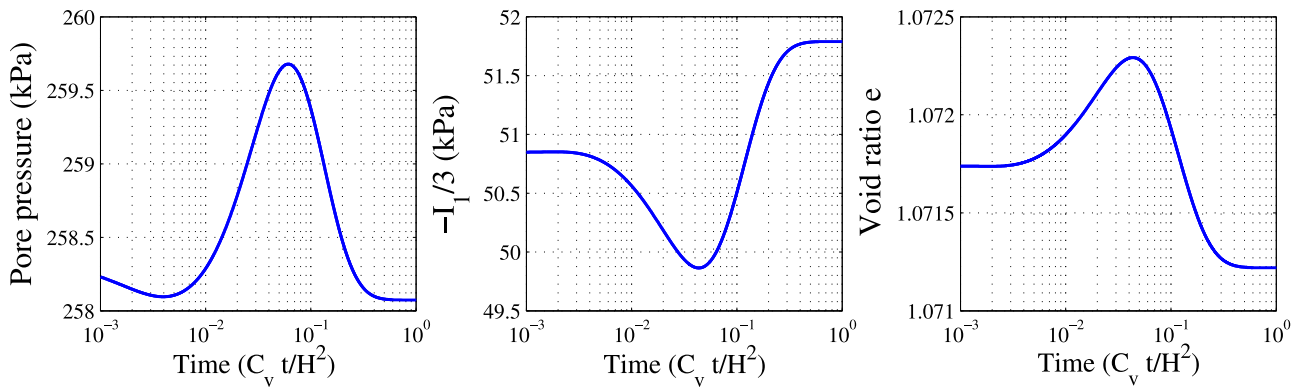


Fig. 18. Process of pore pressure dissipation, mean effective stress increase and void ratio reduction at the typical position A ($x = 750$ m, $z = -6.7$ m) after the fourth layer is built.

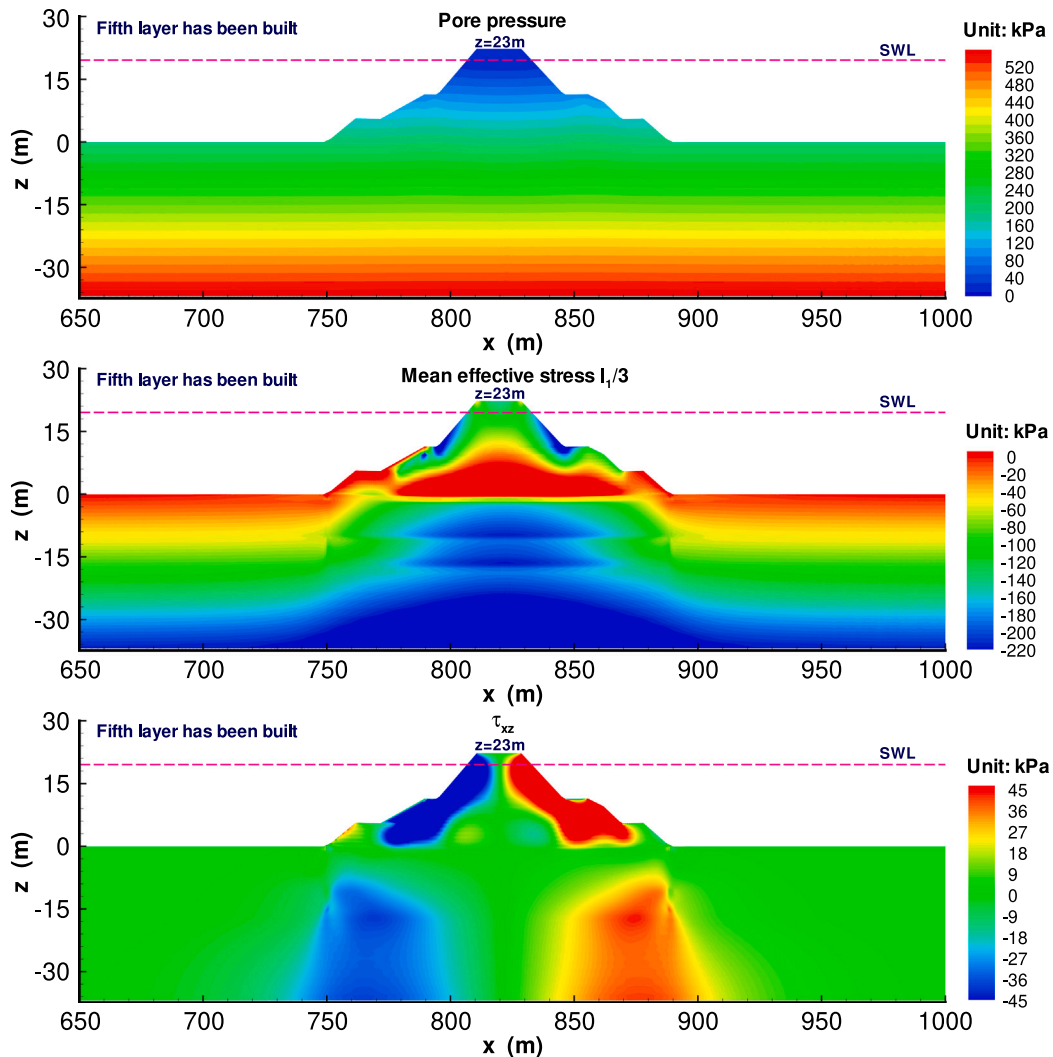
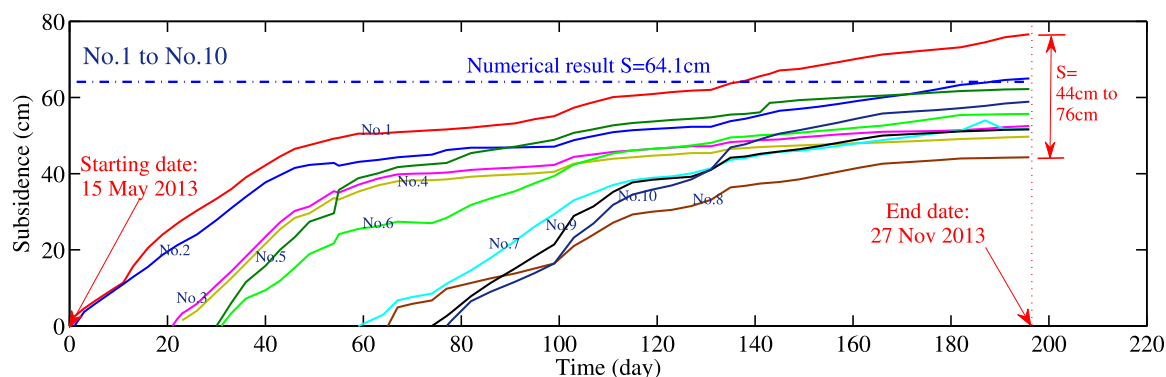


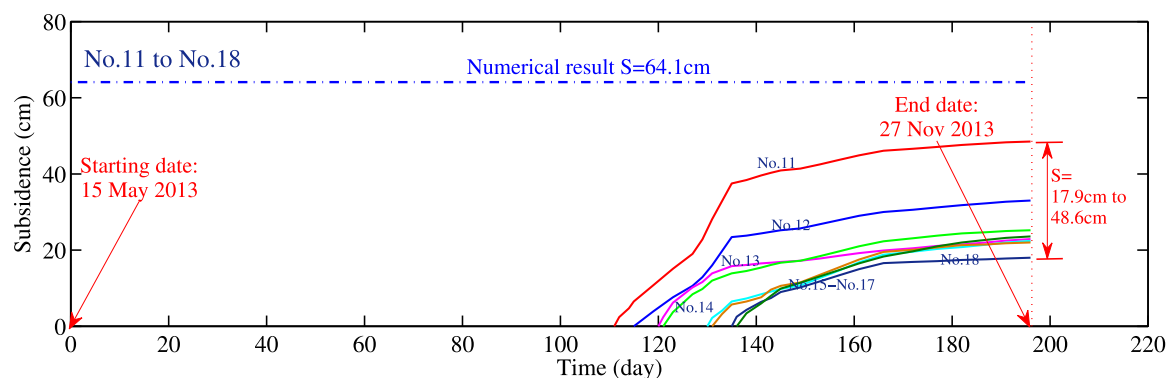
Fig. 19. Distribution of pore pressure, effective stress in the seabed foundation after the fifth layer is built.

the final subsidence predicted by FSSI-CAS 2D is 64.1 cm, which is exactly in the range of the monitoring data at the in-site. The difference to the lower and upper limit of the monitoring data is about -30% and $+13\%$. For a numerical prediction result in practical engineering, this degree of derivation actually is acceptable and commendable. It is indicated that the subsidence of the RM breakwater predicted by FSSI-CAS 2D is reliable, and the integrated numerical model FSSI-CAS 2D is

reliable to predict the consolidation subsidence of offshore structures so long as their foundation soil layers could be relatively accurately divided through the geotechnical survey, as well as appropriate soil constitutive models are used and reliable model parameters for soil layers are calibrated through laboratory tests.



(a) NO.1 to NO.10



(B) NO.11 to NO.18

Fig. 20. Subsidence process of the rubble mound breakwater measured at in-site after construction.

7. Conclusion

In this study, taking the huge rubble mound breakwater in the west part zone at Yantai port as the engineering background, the integrated numerical model FSSI-CAS 2D is adopted to predict the subsidence of the rubble mound breakwater built on the seabed foundation composed by muddy-clay, clay and silty soil layers. In computation, the modified Cambridge soil model and poro-elastic model are used to describe the behavior of the seabed foundation soil layers. One of priorities in this study is that the buoyancy applied on the rubble mounds and its nonlinear variation under Static Water Level (SWL) is taken into consideration in FSSI-CAS 2D. The computational results show that the rubble mound breakwater gradually subsides during the construction period. The final subsidence is predicted as 64.1 cm, which is exactly in the range of monitoring data. The deviation to the lower and upper limit of the in-site monitoring data is about -30% and 13%, respectively. This degree of deviation actually is acceptable for a numerical model when it is applied in engineering practice. Through the analytical and experimental verification, as well as the comparison with in-situ observation data, it is indicated that the integrated numerical model FSSI-CAS 2D is usable for the problems of consolidation, and for the subsidence prediction of structures, and FSSI-CAS 2D has the potential ability to be applied in practical engineering.

It must be noted that there are also several limitations in the present work. Firstly, the randomness in the soil layers distribution in the seabed foundation cannot be considered in computation. Definitely, this randomness also cannot be clearly figured out by engineers due to the fact only limited number of drilling can be performed in the geotechnical survey. Therefore, this limitation is inevitable in numerical modeling. Secondly, several parameters used in computation are not directly measured in laboratory, but estimated based on some

other measured parameters. Thirdly, the building process of the rubble mound breakwater cannot be modeled in FSSI-CAS 2D. The real gradual loading process during the construction period is simplified as five times of transient loading. The above limitations and simplification would have some unquantifiable effect for the prediction result. As a result, the numerical prediction result is impossible to be exactly the same with the in-site observation data.

FSSI-CAS 2D cannot be applied for the problems of wave/current-induced scouring. It only can be applicable for the problems of consolidation, subsidence, dynamics of structures and their foundation under self-weight, ocean wave loading or seismic wave loading. Currently, there are also three aspects that could limit the application potential of FSSI-CAS 2D. Firstly, there is still no graphic user interface developed. As a result, it is a little difficult for new users to use it. Secondly, there is no parallel computation developed, resulting in that a large-scale computation is impossible to be implemented for practical engineering cases. Thirdly, the thermodynamics and the unsaturation of soil cannot be handled so far. These problems can only be solved step by step in the future.

CRediT authorship contribution statement

Jianhong Ye: Conceptualization, Methodology, Formal analysis, Writing, Supervision, Funding acquisition. Kungpeng He: Investigation, Visualization. Lijie Zhou: Investigation, Visualization.

Declaration of competing interest

The authors declare that they have no known competing financial interests or personal relationships that could have appeared to influence the work reported in this paper.

Acknowledgment

Professor Jianhong YE are grateful to the funding support from National Natural Science Foundation of China under project 51879257.

References

- Anderson, K.H., 2009. Bearing capacity under cyclic loading — offshore, along the coast, and on land. The 21st Bjerrum Lecture presented in Oslo, 23 November 2007. *Can. Geotech. J.* 46 (5), 513–535.
- Chan, A.H.C., 1988. A Unified Finite Element Solution to Static and Dynamic Problems of Geomechanics (Ph.D. thesis). University of Wales, Swansea Wales.
- Cheng, A.H.D., Detournay, E., 1988. A direct boundary element method for plane strain poroelasticity. *Int. J. Numer. Anal. Methods Geomech.* 12, 551–572.
- Cryer, C.W., 1963. A comparison of the three-dimensional consolidation theories of Biot and Terzaghi. *Quart. J. Mech. Appl. Math.* XVI (4), 401–412.
- Daigle, H., Worthington, L.L., Gulick, S.P.S., Avendonk, H.J.A.V., 2017. Rapid sedimentation and overpressure in shallow sediments of the Bering Trough, offshore southern Alaska. *J. Geophys. Res. Solid Earth* 122 (4), 2457–2477.
- Fazeres-Ferradosa, T., Taveira-Pinto, F., Romão, X., Vanem, E., Reis, M.T., das Neves, L., 2018. Probabilistic design and reliability analysis of scour protections for offshore windfarms. *Eng. Fail. Anal.* 91, 291–305.
- Fazeres-Ferradosa, T., Welzel, M., Schendel, A., Baelus, L., Santos, P.R., Pinto, F.T., 2020. Extended characterization of damage in rubble mound scour protections. *Coast. Eng.* 158, 103671.
- He, K.P., Huang, T.K., Ye, J.H., 2018. Stability analysis of a composite breakwater at Yantai port, China: An application of FSSI-CAS-2D. *Ocean Eng.* 168, 95–107.
- Hsu, T.J., Sakakiyama, T., Liu, P.L.F., 2002. A numerical model for wave motions and turbulence flows in front of a composite breakwater. *Coast. Eng.* 46, 25–50.
- Jeng, D.S., Ye, J.H., 2012. Three-dimensional consolidation of a porous unsaturated seabed under rubble mound breakwater. *Ocean Eng.* 53, 48–59.
- Karamitros, D.K., Bouckovalas, G.D., Chaloulos, Y.K., 2013. Seismic settlements of shallow foundations on liquefiable soil with a clay crust. *Soil Dyn. Earthq. Eng.* 46, 64–76.
- Konagai, K., Kiyota, T., Suyama, S., Asakura, T., Shibuya, K., Eto, C., 2013. Maps of soil subsidence for Tokyo bay shore areas liquefied in the March 11th, 2011 off the Pacific coast of Tohoku earthquake. *Soil Dyn. Earthq. Eng.* 53, 240–253.
- Li, Y.Z., Ong, M.C., Tang, T., 2020. A numerical toolbox for wave-induced seabed response analysis around marine structures in the OpenFOAM framework. *Ocean Eng.* 195, 106678.
- Liao, C.C., Tong, D.K., Chen, L., 2018. Pore pressure distribution and momentary liquefaction in vicinity of impermeable slope-type breakwater head. *Appl. Ocean Res.* 78, 290–306.
- Mandel, J., 1953. Consolidation des sols (étude mathématique). *Géotechnique* 3, 287–299.
- Miyamoto, J., Sassa, S., Sekiguchi, H., 2004. Progressive solidification of a liquefied sand layer during continued wave loading. *Géotechnique* 54 (10), 617–629.
- Nakai, T., Matsuoka, H., 1986. A generalized elastoplastic constitutive model for clay in three dimensional stresses. *Soil Found.* 26 (3), 81–98.
- Setan, H., Othman, R., 2006. Monitoring of offshore platform subsidence using permanent GPS stations. *J. Global Position. Syst.* 5 (1), 17–21.
- Shen, J.H., Wu, H.C., Zhang, Y.T., 2017. Subsidence estimation of breakwater built on loosely deposited sandy seabed foundation: Elastic model or elasto-plastic model. *Int. J. Naval Arch. Ocean Eng.* 9, 418–428.
- Sumer, B.M., Ansal, A., Cetin, K.O., Damgaard, J., Gunbak, A.R., Hansen, N.E.O., Sawicki, A., Synolakis, C.E., Yalciner, A.C., Yuksel, Y., Zen, K., 2007. Earthquake-induced liquefaction around marine structures. *J. Waterw. Port Coast. Ocean Eng.* 133 (1), 55–62.
- Terzaghi, K., 1925. *Erdbaumechanik auf Bodenphysikalischer Grundlage*. F. Dutticke, Vienna.
- Verdugo, R., Gonzalez, J., 2015. Liquefaction-induced ground damages during the 2010 Chile earthquake. *Soil Dyn. Earthq. Eng.* 79, 280–295.
- Ye, J.H., 2012a. Numerical Analysis of Wave-Seabed-Breakwater Interactions (Ph.D. thesis). University of Dundee, Dundee, UK.
- Ye, J.H., 2012b. Numerical modelling of consolidation of 2-D porous unsaturated seabed under a composite breakwater. *Mechanika* 18 (4), 373–379.
- Ye, J.H., Jeng, D.-S., Chan, A.H.C., 2012. Consolidation and dynamics of 3D unsaturated porous seabed under rigid caisson breakwater loaded by hydrostatic pressure and wave. *Sci. China* 55 (8), 2362–2376.
- Ye, J.H., Jeng, D.S., Chan, A.H.C., Wang, R., Zhou, C.Q., 2017. 3D integrated numerical model for fluid-structures-seabed interaction (FSSI): Loosely deposited seabed foundation. *Soil Dyn. Earthq. Eng.* 92, 239–252.
- Ye, J.H., Jeng, D.-S., Liu, P.L.-F., Chan, A.H.C., Wang, R., Zhu, C.-Q., 2014. Breaking wave-induced response of composite breakwater and liquefaction of seabed foundation. *Coast. Eng.* 85, 72–86.
- Ye, J.H., Jeng, D.-S., Wang, R., Zhu, C.-Q., 2013. Validation of a 2D semi-coupled numerical model for fluid-structures-seabed interaction. *J. Fluids Struct.* 42, 333–357.
- Ye, J.H., Jeng, D.-S., Wang, R., Zhu, C.-Q., 2015. Numerical simulation of wave-induced dynamic response of poro-elasto-plastic seabed foundation and composite breakwater. *Appl. Math. Model.* 39, 322–347.
- Ye, J.H., Wang, G., 2015. Seismic dynamics of offshore breakwater on liquefiable seabed foundation. *Soil Dyn. Earthq. Eng.* 76, 86–99.
- Ye, J.H., Wang, G., 2016. Numerical simulation of the seismic liquefaction mechanism in an offshore loosely deposited seabed. *Bull. Eng. Geol. Environ.* 75 (3), 1183–1197.
- Zienkiewicz, O.C., Chan, A.H.C., Pastor, M., Schrefler, B.A., Shiomi, T., 1999. *Computational Geomechanics with Special Reference to Earthquake Engineering*. John Wiley and Sons, England.
- Zienkiewicz, O.C., Chang, C.T., Bettess, P., 1980. Drained, undrained, consolidating and dynamic behaviour assumptions in soils. *Géotechnique* 30 (4), 385–395.